Temperature dependence of carbon nanofiber resistance

2010 Nanotechnology 21 265707

(http://iopscience.iop.org/0957-4484/21/26/265707)

Nanotechnology **21** (2010) 265707 (5pp) doi:10.1088/0957-4484/21/26/265707

Temperature dependence of carbon nanofiber resistance

Toshishige Yamada[1], **Hisashi Yabutani, Tsutomu Saito and Cary Y Yang**

Center for Nanostructures, Santa Clara University, 500 El Camino Real, Santa Clara, CA 95053, USA

E-mail: tyamada@scu.edu

Received 4 February 2010, in final form 22 April 2010
Published 10 June 2010
Online at stacks.iop.org/Nano/21/265707

Abstract
Transport properties under current stress are examined for a carbon nanofiber (CNF) on an insulating substrate between tungsten-deposited gold electrodes. The temperature dependence of CNF resistance is determined based on our previously reported heat transport model. The measured devices exhibit a thermal activation behavior, suggesting transport in a disordered medium. The extracted activation energies fall within the 22–35 meV range.

1. Introduction

Carbon nanofibers (CNFs) belong to the family of covalent nanocarbon materials and are promising candidates for next-generation on-chip interconnect materials [1–6]. CNFs are immune to electromigration, resulting in much higher current capacity than Cu [7, 8], and are easily obtainable with aligned vertical growth at moderately low temperatures, which are suited for on-chip via interconnect applications [4]. Transport properties of this material at elevated temperatures are of scientific and technological interest. While it is possible to perform electrical measurements on CNFs at elevated temperatures, various transport mechanisms within the test structure needs to be differentiated. It is nontrivial to study a single CNF since it has an extremely small heat capacity and maintaining thermal equilibrium is highly challenging. One way to overcome this problem is to embed a parallel array of CNFs in an insulator inside a via hole so that the system heat capacity will be effectively increased [9]. Using this approach, thermally activated transport, typical of transport in disordered media [10], was observed [9]. In this work, we raise the temperature of a single CNF using Joule heating, which is placed horizontally on metal electrodes on an insulating substrate. Current is progressively applied and the total resistance of a CNF between two electrodes is measured after and during each current stress cycle, until breakdown occurs. Total resistance does not change if the measurement is performed *after* completion of a stress cycle (with the CNF cooled down to ambient temperature). But the average resistance obtained *during* each cycle decreases with increasing the stress current from one cycle to the next (with the CNF subject to increasing Joule heating). We convert stress current to CNF average temperature using our previously reported heat transport model [11], and obtain conductivity as a function of temperature.

[1] Author to whom any correspondence should be addressed.

2. Current stress experiment

A multi-wall carbon nanotube (CNT) consists of parallel rolled graphene sheets with a diameter ranging from several nm to several 100 nm. Thus as in a single-wall CNT, the interior is hollow. A carbon nanofiber (CNF) also has parallel rolled graphene sheets as the outer layers, but has a stacked-cup structure in the interior which is no longer hollow. Adjacent cups are separated by ∼0.5 nm, thus electron transport occurs largely along the outer graphene layers. A transmission electron micrograph (TEM) image of a CNF is shown in figure 1. In CNTs, if the structure is free of defects and impurities, transport is ballistic in low fields with conductance equal to a multiple of quantum conductance $G_Q = q^2/h$ (q is the unit electronic charge and h the Planck constant), but classical (ohmic) in high fields [12], since electrons can gain sufficiently high kinetic energy in high fields and emit phonons (inelastic scattering) [13]. Our CNFs are metallic [14], but contain impurities and/or lattice defects in the outer graphene layers and in the stacked-cup layers, giving rise to electron traps [9]. As far as electrical transport properties are concerned, typical metals are rather immune to impurities/defects due to their extremely large

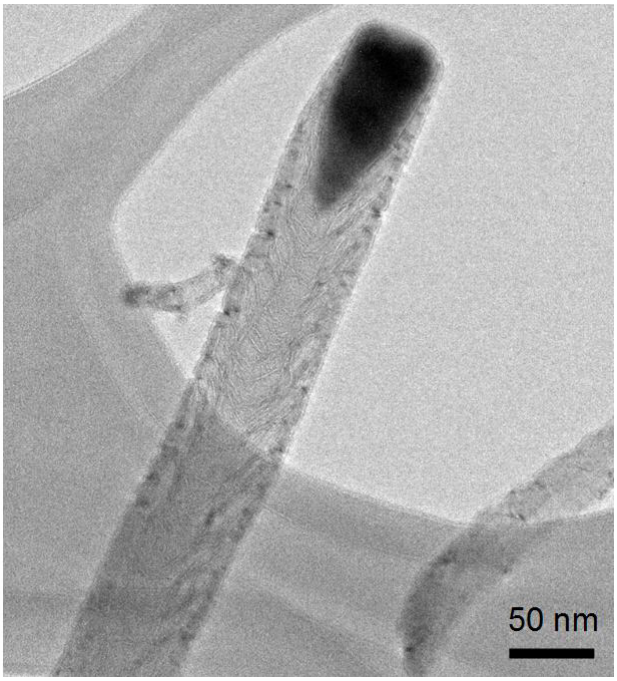

Figure 1. TEM image of a CNF using the plasma-enhanced chemical vapor deposition method with Ni catalyst.

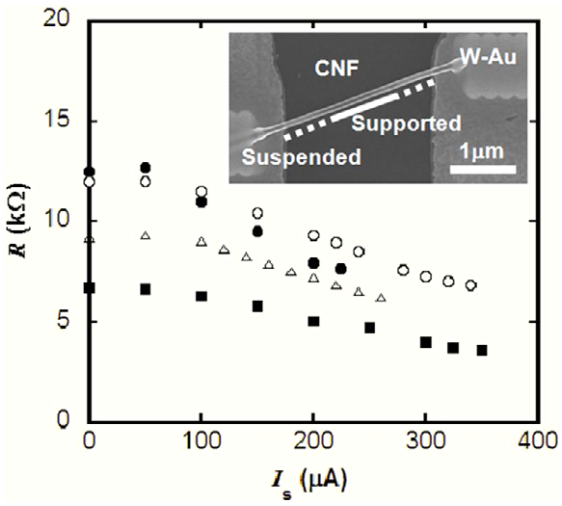

Figure 2. Total resistance R as a function of stress current I_s, averaged over each stress cycle for four devices (filled circle, open circle, triangle, and square). $I_s = 0$ corresponds to the ambient temperature data. Inset: SEM image of the CNF device. Supported segments are indicated by solid lines and suspended segments by broken lines.

electron density of states at the Fermi level, but CNFs or CNTs approach a semi-metal 2D graphene in the large diameter limit, and their counterpart is much smaller than that in typical metals [15], resulting in vulnerability to disorder. In our CNFs, transport is largely dictated by disorder [10]. CNFs used in these measurements were grown using the plasma-enhanced chemical vapor deposition method with Ni catalyst [12]. The diameters of these CNFs range from 90 to 156 nm. Using a focused ion beam, tungsten (W) was deposited onto the CNF at pre-fabricated gold (Au) electrode contacts [8]. Figure 2 inset shows a scanning electron microscope (SEM) image of such a CNF with W–Au electrodes. All the measurements are performed in ambient. Total resistance is in the kΩ range. The current–voltage (I–V) behavior is linear and the electrode contacts are robust after W deposition, minimizing the unwanted contact effects [8]. From four-point probe measurements, the average resistivity for *unstressed* CNF is determined to be $\rho_{\mathrm{CNF}} = 1.3 \times 10^{-5}\ \Omega$ m [17]. Using a typical diameter $d \sim 100$ nm and length $L \sim 4\ \mu$m, we obtain a CNF resistance $R_{\mathrm{CNF}} = \rho_{\mathrm{CNF}} \times L/\pi(d/2)^2 = 6.4\ \mathrm{k}\Omega$ at 300 K. The total resistance in figure 2 is in this range, indicating that contact resistance R_c satisfies $R_c < R_{\mathrm{CNF}}$ (or $R_c \ll R_{\mathrm{CNF}}$) consistently, and thus it is reasonable to neglect R_c in our analysis.

Stress current is applied progressively, i.e. in the first cycle, a small constant current is applied for 3 min, and in the second cycle, a larger constant current is applied for another 3 min, etc. When resistance is measured *after* each stress cycle using much smaller current and voltage, the CNF is cooled down to ambient temperature. Total resistance measured between the two electrodes changes very little, by at most 20% after multiple stress cycles [8]. This behavior is in sharp contrast with results for current stressing of CNF drop-casted on Au electrodes, where the total resistance drops by orders of magnitude until breakdown, largely due to contact resistance reduction [8]. This suggests that for CNF between W–Au electrodes, the contact resistance is not only unaffected by current stressing, but also small relative to CNF resistance. When the average resistance is measured *during* each stress cycle, it decreases from one cycle to the next. Figure 2 shows the total resistance as a function of stress current for four different devices, averaged over each stress cycle. Since the device is subject to Joule heating during current stress, and since its average temperature must increase with increasing stress current, the total resistance must then decrease with elevated temperature. The stress current versus temperature behavior is examined in section 3.

3. Conversion of stress current to average temperature

Our one-dimensional heat transport model [12] takes into account Joule heat generation by stress current, dissipation to SiO_2 substrate/electrode, and diffusion, as given by

$$\mathrm{d}^2\Delta T(x)/\mathrm{d}x^2 - a(x)^2\Delta T(x) = -bJ^2. \qquad (1)$$

$\Delta T(x) = T(x) - T_0$, where T_0 is ambient temperature, J is the current density and $b = 1/(\kappa\sigma)$, where κ is the thermal conductivity and σ is the electrical conductivity of the CNF. $a(x)$ is a dissipation factor modeled by a piecewise function. a_f is for the suspended segment, a_s is for the SiO_2 substrate supported segment, and a_e is for the W–Au electrode. $a_f \ll a_s \ll a_e$ is expected. The analytical solution of $\Delta T(x)$ is connected at the junction with different as, by demanding continuous ΔT and $\mathrm{d}\Delta T/\mathrm{d}x$ [11]. Suspended/supported segments are identified by analyzing SEM image contrast [11].

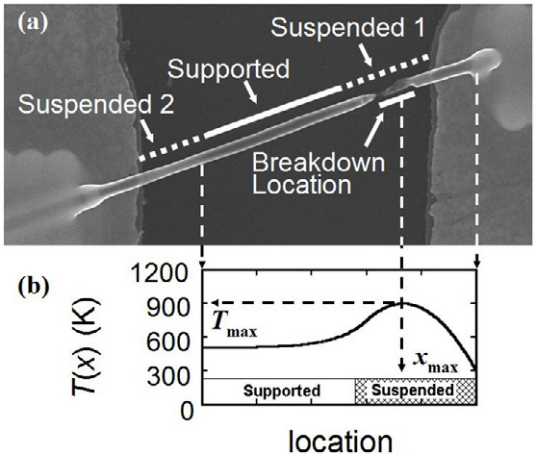

Figure 3. (a) SEM image of the same device shown in figure 2(a) after breakdown. Supported segments are indicated by solid lines and suspended segments by broken lines. (b) Calculated temperature profile $T(x)$.

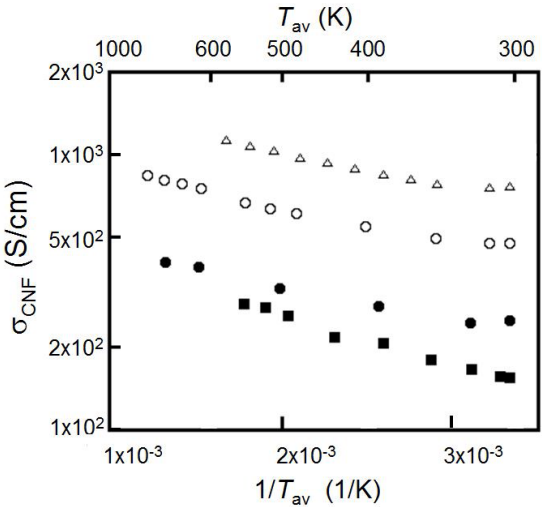

Figure 4. Conductivity σ_{CNF} as a function of inverse average temperature $1/T_{\mathrm{av}}$ for the same four devices (the same symbols assigned) as in figure 2.

In figure 3(a), the device has suspended 1 (bright), supported (dark) and suspended 2 (bright) segments [18]. Breakdown occurred in the suspended 1 segment, where the highest temperature T_{max} just exceeded the threshold temperature T_{th}. Thus, we consider only suspended 1 and supported segments for average temperature determination.

Setting $a_{\mathrm{f}} \sim 0$ and $a_{\mathrm{e}} \sim \infty$ in our model, we fit the only unknown parameter a_{s} to recover $T_{\mathrm{max}} = T_{\mathrm{th}}$ at measured J_{max}. Hata *et al* reported that the weight reduction for a single-walled carbon nanotube forest (film) occurred in the 550–750 °C range in the thermo-gravimetric measurement [19]. We choose $T_{\mathrm{th}} =$ 900 K, which is close to the onset of breakdown as in our previous analysis [7, 11]. For the CNF in figure 3(a), a_{s} is found to be 3.6 $\mu\mathrm{m}^{-1}$ and $T(x)$ at J_{max} is calculated and shown in figure 3(b). $T(x)$ is parabolic in the suspended segment due to minimal heat dissipation, while $T(x)$ is constant in the supported segment due to negligible diffusion. The T_{max} location compares well with the measurement. Since $\Delta T(x) \propto J^2$ as shown in equation (1), spatially averaged temperature $\Delta T_{\mathrm{av}}(J)$ is given by $\Delta T_{\mathrm{av}}(J_{\mathrm{max}})J^2/J_{\mathrm{max}}^2$. This is how we relate stress current to average temperature.

The stress current in figure 2 is now converted to temperature. We assume that the CNF contribution to total resistance is dominant in the W–Au electrode as suggested earlier, and evaluate CNF conductivity σ_{CNF} using Ohm's law with the length and cross-sectional area. In figure 4, an Arrhenius plot of σ_{CNF} versus $1/T_{\mathrm{av}}$ is shown for the four devices. This behavior is analyzed using the relation

$$\sigma_{\mathrm{CNF}} = \sigma_0 \exp(-E_{\mathrm{a}}/k_{\mathrm{B}}T), \tag{2}$$

where k_{B} is the Boltzmann constant, σ_0 is a device-dependent parameter, and E_{a} is the activation energy. From equation (2), E_{a} is estimated to range from 22 to 35 meV.

The behavior of $\sigma_{\mathrm{CNF}}(1/T)$ in figure 4 appears for carrier transport in disordered media, which is in sharp contrast to the usual behavior of metals showing lower conductivity at higher temperature [10]. Our CNFs are metallic [17], but contain impurities and/or lattice defects in the outer graphene layers, giving rise to electron traps [9] due to the small Fermi density of states. Joule heating serves to de-trap trapped electrons through thermal activation, creating additional carriers. This assertion is supported by the Arrhenius behavior for all four devices shown in figure 4. Accordingly, more electrons participate in transport as the CNF temperature increases, resulting in a decrease in resistance. Since resistance at ambient temperature is unaffected before and after current stress, electrons must be recaptured by traps as the temperature returns to ambient. Thus this trapping/de-trapping process is completely reversible. Figure 4 reveals a significant variation in σ_0 (vertical axis intercept) but similar activation energies E_{a} (slopes). Since CNFs were synthesized using the same growth conditions, defects themselves should be the same (sharing similar E_{a}s). However, their density could be different from device to device because of the large CNF diameters, ranging from 90 to 156 nm, which explains the significant variation in σ_0.

Carbon graphite fiber conductivity ranges between 500 (as grown) and 20 000 (high-temperature treated, close to ideal graphite) S cm^{-1} [20]. Our measured CNF conductivity at 300 K given in figure 4 ranges from 200 to 900 S cm^{-1}, consistent with transport in a disordered medium. In our previous work [21], we reported that breakdown occurs along the stacked-cone surface, originating from void formation and growth as a result of Joule heating. If the temperature is elevated but stays below the threshold temperature, it is expected that the morphology change, if any, is reversible, because the total resistance comes back to its original value.

4. Comparison to previous study

In our previous study [16], we examined transport in vertically aligned CNF arrays in a via interconnect structure. The CNF arrays were grown on a Ti underlayer as the as-grown electrode, with a Ti/Pt contact pad deposited on top

after oxide encapsulation. I–V measurement was performed in the temperature range from 4.2 to 350 K. The entire structure was subject to heating/cooling while the temperature was measured. The measured conductivity was fitted to $\sigma_{\mathrm{CNF}} = \sigma_0 \exp(-E_a/k_B T) + \sigma_1$. The term σ_1 accounted for the finite residual contribution in the limit of $T \to 0$, and σ_{CNF} was shown to reduce to equation (2) at or above ambient temperature. Using this fitting equation, the activation energy E_a was extracted to be 26 meV [9]. The present activation energy range of 22–35 meV is consistent with this value. Despite the obvious differences in device structure, temperature range, and temperature determination, the similarity in E_a is remarkable but expected as both systems share the same thermal activation process. Since defects or impurities are unavoidable in CNFs with diameters ~100 nm, it is meaningful to elucidate the CNF transport properties at elevated temperatures and in high fields (high current densities), in assessing its potential in interconnect as well as other applications. The reversible temperature-dependent transport in CNFs may also be suitable for thermistor applications.

As discussed in [3], carbon nanotubes (CNTs) show the opposite trend, i.e. the conductivity decreases with temperature, because phonon scattering dominates at higher temperature and the influence of impurities/defects is not significant. In growing a very narrow CNT, impurities/defects are much less likely to be present than in a much wider CNF. Some such defects are visible in the TEM image shown in figure 1. Our observation is consistent with the expectation that phonon-limited transport occurs in CNTs and disorder-limited transport in CNFs due to the presence of large numbers of defects.

As long as breakdown does not occur, the change in resistance with temperature is reversible. In our previous work [21], we reported that breakdown occurs along the stacked-cone surface, originating from void formation and growth as a result of Joule heating. If the temperature is elevated but stays below the breakdown threshold, it is expected that the morphology change, if any, is reversible, since the total resistance returns to its ambient value upon cooling.

Tsuzuku and Saito [22] showed that the activation energy for thermal depinning of dislocations in graphite ranges between 40 meV and 30 meV before and after bromination, respectively, and 6 meV for the boronates. Our estimated activation energies in the 22–35 meV range are consistent with these values and point to similar defect origins in graphitic materials. The reversible and temperature-dependent conductivity may lead to potential applications as a thermistor. Also, such behavior is critical in thermal management considerations during the design process for using CNFs as on-chip interconnects.

5. Conclusion

Transport properties of a horizontally placed CNF connected between W–Au electrodes, one of the simplest test structures for interconnect applications, are studied. The temperature dependence of CNF resistance is determined based on our previously developed heat transport model [11]. CNF resistance decreases with increasing temperature, and the CNF conductivity has an Arrhenius behavior, with extracted activation in the 22–35 meV range, consistent with the 26 meV we extracted previously using a vertical via structure [9].

Acknowledgments

This work was supported by the United States Army Space and Missile Defense Command (SMDC) and carries Distribution Statement A, approved for public release, distribution unlimited.

References

[1] Nihei M, Kawabata A, Kondo D, Horibe M, Sato S and Awano Y 2005 Electrical properties of carbon nanotube bundles for future via interconnects *Japan. J. Appl. Phys.* **44** 1626

[2] Zhang L, Austin D, Merkulov V I, Meleshko A V, Klein K L, Guillorn M A, Lowndes D H and Simpson M L 2004 Four-probe charge transport measurements on individual vertically aligned carbon nanofibers *Appl. Phys. Lett.* **84** 3972

[3] Kuroda M A, Cangellaris A and Leburton J P 2005 Nonlinear transport and heat dissipation in metallic carbon nanotubes *Phys. Rev. Lett.* **95** 266803

[4] Ngo Q, Cassell A M, Austin A J, Li J, Krishnan S, Meyyappan M and Yang C Y 2006 Characteristics of aligned carbon nanofibers for interconnect via applications *IEEE Electron Device Lett.* **27** 221

[5] Plombon J J, O'Brien K P, Gstrein F, Dubin V M and Jiao Y 2007 High-frequency transport electrical properties of individual and bundled carbon nanotubes *Appl. Phys. Lett.* **90** 063106

[6] Pop E, Mann D, Goodson K and Dai H 2007 Electrical and thermal transport in metallic single-wall carbon nanotubes on insulating substrates *J. Appl. Phys.* **101** 093710

[7] Kitsuki H, Yamada T, Fabris D, Jameson J R, Wilhite P, Suzuki M and Yang C Y 2008 Length dependence of current-induced breakdown of carbon nanofibers *Appl. Phys. Lett.* **92** 173110

[8] Saito T, Yamad T, Fabris D, Kitsuki H, Wilhite P, Suzuki M and Yang C Y 2008 Improved contact for thermal and electrical transport in carbon nanofiber interconnects *Appl. Phys. Lett.* **93** 102108

[9] Ngo Q, Yamada T, Suzuki M, Ominami Y, Cassell A M, Li J, Meyyappan M and Yang C Y 2007 Structural and electrical characterization of carbon nanofibers for interconnect via applications *IEEE Trans. Nanotechnol.* **6** 688

[10] Ando T, Fowler A B and Stern F 1982 Electronic properties of two-dimensional systems *Rev. Mod. Phys.* **54** 437

[11] Yamada T, Saito T, Fabris D and Yang C Y 2009 Electrothermal analysis of breakdown in carbon nanofiber interconnects *IEEE Electron Device Lett.* **30** 469

[12] Beenakker C W J and van Houten H 1991 *Solid State Physics* vol 44, ed H Ehrenreich and D Turnbull (San Diego, CA: Academic)

[13] Yamada T and Sone J 1989 High-field electron transport in quantum wires studied by solution of the Boltzmann equation *Phys. Rev.* B **40** 6265

[14] Dresselhaus M S and Endo M 2001 Relation of carbon nanotubes to other carbon nanomaterials *Carbon Nanotubes: Synthesis, Structure, Properties, and Applications* ed R E Smalley, M S Dresselhaus, G Dresselhaus and Ph Avouris (Boston, MA: Springer)

[15] Wallace P R 1947 The band theory of graphite *Phys. Rev.* **71** 622
[16] Cruden B A, Cassell A M, Ye Q and Meyyappan M 2003 Reactor design considerations in the hot filament/direct current plasma synthesis of carbon nanofibers *J. Appl. Phys.* **94** 4070
[17] Yamada T, Saito T, Suzuki M, Wilhite P, Sun X, Akhavantafti N, Fabris D and Yang C Y 2010 Tunneling between carbon nanofiber and gold electrodes *J. Appl. Phys.* **107** 044304
[18] Suzuki M, Yamada T and Yang C Y 2007 Monte Carlo simulation of scanning electron microscopy bright contrast images of suspended carbon nanofibers *Appl. Phys. Lett.* **90** 083111
[19] Hata K, Futaba D N, Mizuno K, Namai T, Yumura M and Iijima S 2004 Water-assisted highly efficient synthesis of impurity-free single walled carbon nanotubes *Science* **306** 1362
[20] Heremans J 1985 Electrical conductivity of vapor-grown carbon fibers *Carbon* **23** 431
[21] Suzuki M, Ominami Y, Ngo Q, Yang C Y, Cassell A M and Li J 2007 Current-induced breakdown of carbon nanofibers *J. Appl. Phys.* **101** 114307
[22] Tuzuku T and Saito M 1967 Impurity dope effects on an elasticity of graphite *Japan. J. Appl. Phys.* **6** 54